^{18}F-GP1, a Novel PET Tracer Designed for High-Sensitivity, Low-Background Detection of Thrombi

Jessica Lohrke[1], Holger Siebeneicher[1], Markus Berger[1], Michael Reinhardt[1], Mathias Berndt[2], Andre Mueller[2], Marion Zerna[2], Norman Koglin[2], Felix Oden[2], Marcus Bauser[1], Matthias Friebe[2], Ludger M. Dinkelborg[2], Joachim Huetter[1], and Andrew W. Stephens[2]

[1]*Bayer AG, Drug Discovery, Berlin, Germany; and* [2]*Piramal Imaging GmbH, Berlin, Germany*

Thromboembolic diseases such as myocardial infarction, stroke, transient ischemic attacks, and pulmonary embolism are major causes of morbidity and mortality worldwide. Glycoprotein IIb/IIIa (GPIIb/IIIa) is the key receptor involved in platelet aggregation and is a validated target for therapeutic approaches and diagnostic imaging. The aim of this study was to develop and characterize a specific small-molecule tracer for PET imaging that binds with high affinity to GPIIb/IIIa receptors and has suitable pharmacokinetic properties to overcome limitations of previous approaches. **Methods:** Binding of ^{18}F-GP1 to GPIIb/IIIa receptors was investigated in competition binding assays and autoradiography using a fresh cardiac thrombus from an explanted human heart. The clot-to-blood ratio for ^{18}F-GP1 was investigated by an in vitro blood flow model. Biodistribution and thrombus detection was investigated in cynomolgus monkeys after insertion of a roughened catheter into either the vena cava or the aorta. **Results:** ^{18}F-GP1 is an ^{18}F-labeled small molecule for PET imaging of thrombi. The half maximal inhibitory concentration of ^{18}F-GP1 to GPIIb/IIIa was 20 nM. ^{18}F-GP1 bound to thrombi with a mean clot-to-blood ratio of 95. Binding was specific and can be displaced by excess nonradioactive derivative. Binding was not affected by anticoagulants such as aspirin or heparin. ^{18}F-GP1 showed rapid blood clearance and a low background after intravenous injection in cynomolgus monkeys. Small arterial, venous thrombi, thrombotic depositions on damaged endothelial surface, and small cerebral emboli were detected in vivo by PET imaging. **Conclusions:** ^{18}F-GP1 binds specifically with high affinity to the GPIIb/IIIa receptor involved in platelet aggregation. Because of its favorable preclinical characteristics, ^{18}F-GP1 is currently being investigated in a human clinical study.

Key Words: imaging; platelets; embolism; thrombosis; glycoproteins

J Nucl Med 2017; 58:1094–1099
DOI: 10.2967/jnumed.116.188896

Venous and arterial thrombi play an important role in various vascular pathologies such as myocardial infarction, stroke, transient ischemic attacks, deep vein thrombosis (DVT), and pulmonary embolism (PE) (*1*). These thromboembolic diseases are a major cause of morbidity and mortality worldwide. Currently available diagnostic techniques of thrombus imaging rely on different modalities depending on the vascular territory. For example, ultrasound is used for detection of DVT (*2*) and carotid stenosis (*3*), transesophageal echocardiography and contrast-enhanced MRI are used for cardiac chamber clots (*4*), and contrast medium–enhanced CT pulmonary angiography has become the gold standard for the detection of PE (*5,6*).

Limitations remain in the tests to diagnose venous clots in DVT and PE; an agent that could visualize both would be valuable (*7*). In addition, standard imaging modalities generally do not allow for reliable discrimination between fresh unstable thrombi and chronic organized thrombi. Imaging of DVT with ultrasound is limited to proximal large vein disease and is unable to distinguish active thrombotic processes in the context of recurrent disease, nor does it have high sensitivity in distal or small vessel disease (*8*). CT pulmonary angiography has demonstrated acceptable sensitivity for PE, although the sensitivity decreases in the acute setting and as the location of the PE becomes more distal (*9*). Underdiagnosis of PE remains a problem as evidenced by the fact that approximately 30% of hospital deaths are complicated by unsuspected PE (*10*).

As a result of arterial thrombi, every year worldwide about 33 million patients experience a new or a recurrent stroke. A highly sensitive molecular imaging approach could potentially identify activated platelets in the presence of atherosclerotic plaques, a harbinger of thromboembolic events. Current imaging modalities rely on structural characteristics, such as vascular flow impairment, and do not address the critical molecular components of the thrombus.

To overcome these diagnostic limitations, new molecular targets and imaging approaches need to be explored. The glycoprotein IIb/IIIa (GPIIb/IIIa) receptor has historically represented an interesting target for drug development because it is a key player in the thrombus formation. Activated platelets express a high number of this receptor (40,000–80,000/platelet) (*11*). GPIIb/IIIa is a member of the integrin family of cell surface proteins and also known as $\alpha_{IIb}\beta_3$. It undergoes allosteric activation on stimulation of the platelet by a variety of agents (e.g., thrombin, adenosine diphosphate, thromboxane). In a growing thrombus, the key step of platelet aggregation is characterized by the binding of activated GPIIb/IIIa to blood fibrinogen domains containing the arginine-glycine-aspartic acid (RGD) motif, which results in crosslinking. The design and development of glycoprotein IIb/IIIa inhibitors has attracted a considerable amount of interest in pharmacologic research with respect to antiplatelet and antithrombotic activity (*12–17*). GPIIb/IIIa antagonists are commercially available, for example, abciximab (ReoPro, Centocor; Eli Lilly), eptifibatide (Integrilin; GlaxoSmithKline), and tirofiban (Aggrastat; Correvio International Sarl). Tirofiban and eptifibatide are both synthetic RGD peptidomimetics.

Several radiotracer-based diagnostic approaches have been explored previously including targeting of GPIIb/IIIa (*18*). For example,

Received Dec. 22, 2016; revision accepted Mar. 2, 2017.
For correspondence or reprints contact: Andrew W. Stephens, Piramal Imaging GmbH, Tegeler Strasse 6-7, 13353 Berlin, Germany.
E-mail: andrew.stephens@piramal.com
Published online Mar. 16, 2017.

^{99m}Tc-labeled peptide apcitide (^{99m}Tc-Acutect; Diatide, Inc.) (*19*) contains an RGD-binding motif and was developed as a SPECT tracer for the detection of DVT. It received Food and Drug Administration approval for this indication but was later abandoned. ^{99m}Tc-Fab against D-Dimer progressed to phase 2 (*20,21*), and preclinical studies with ^{64}Cu-labeled peptides binding to fibrin have recently been described (*22*). The main limitations of agents previously investigated in the clinic were low target-to-background ratios, slow clearance, and inability to distinguish acute versus chronic disease (*18*).

The aim of this study was to develop and characterize a novel small molecule for thrombus PET imaging that has a high affinity to GPIIb/IIIa receptors as well as low background and rapid blood clearance. The preclinical results from an ^{18}F-labeled fiban-class ligand called ^{18}F-GP1 are presented here.

MATERIALS AND METHODS

Synthesis of ^{18}F-GP1

^{18}F-GP1 was synthesized by nucleophilic radiofluorination starting from the protected tosylate precursor. The radiolabel was introduced directly before deprotection of the precursor molecule and subsequent purification (Fig. 1).

In Vitro Characterization of ^{19}F-GP1 and ^{18}F-GP1

GPIIb/IIIa Binding Assay. The half maximal inhibitory concentration (IC_{50}) value of the nonradioactive ^{19}F-GP1 was determined by an in vitro competition assay using microtiter plates coated 48 h with purified human GPIIb/IIIa (5 μg/mL; Enzyme Research Laboratories) in phosphate-buffered saline. The nonspecific antibody binding sites were blocked (Roti-Block; Roth). The plates were incubated with 30 nM ^{3}H-elarofiban (289 GBq/mmol; Bayer Isotope Chemistry) and a dilution series of ^{19}F-GP1 ranging from 0.1 to 2,000 nM in quadruplicate. After 60-min incubation, the plates were washed 3 times with 200 μL of phosphate-buffered saline/well. The wells were filled with 140 μL of scintillation cocktail (Microscint40; Perkin-Elmer). After being shaken for 15 min, plates were measured using a TopCount-NXTv2.13 (Perkin-Elmer). The resulting IC_{50} value represents the mean of 3 independent assays. The platelet aggregation assay was performed as described previously (*23*). Human platelet-rich plasma was investigated after stimulus of adenosine diphosphate and platelet clumping recorded as a dynamic measure.

Autoradiography of Explanted Human Thrombus. Binding of ^{18}F-GP1 to a human thrombus was investigated by autoradiography on a cardiac thrombus from an explanted human heart (gift from the Herz- und Diabeteszentrum, Bad Oeynhausen, Germany). The fresh thrombus from the right ventricle was embedded in Tissue-Tek, and 18-μm cryosections were incubated with ^{18}F-GP1 (50 Bq/μL in 4-(2-hydroxyethyl)piperazine-1-ethanesulfonic acid [HEPES]), 0.1% bovine serum albumin, 100 μL per slice), for 1 h at room temperature, rinsed 3 times with HEPES, and left over night for exposure on BAS-SR Imaging plates (Fuji). A competition experiment was performed by adding an excess of tirofiban (0.5 μg/mL; Sigma) to the ^{18}F-GP1 solution. CD41 (GPIIb) staining was performed with the anti-CD41 antibody from Abcam (ab11024) with the AP-fast red detection system.

In Vitro Blood Flow Model. The binding of ^{18}F-GP1 to thrombi was investigated in an in vitro blood flow model, modified from the method described by Sukavaneshvar (*24*). An open tube set consisting of tygon-tubes (R-1000; inner diameter, 3.2 mm), an open reservoir, and a chamber made of a piece of polyethylene tube (PE160p; Intramedic) was used. The chamber contained a loop with a roughened nylon fishing line for thrombus formation (thrombogenic surface prepared with sandpaper). A peristaltic pump was used for blood circulation. The flow in the middle of the thrombus chamber was adjusted to 70–90 cm per second, monitored by an ultrasound-Doppler measurement. Ten milliliters of fresh blood were taken from a volunteer using citrate tubes (S-Monovette; Sarstedt) and immediately laid into an incubator at a temperature of 37°C (mini-Therm; Heraeus). The thrombus formation was initiated by the addition of 0.75 mL of a 2% $CaCl_2$ solution in the 15-mL tube set (final concentration, 10 mM $CaCl_2$). After 7 min of thrombus formation, ^{18}F-GP1 (0.5–1.0 MBq) was added. The recalcified blood and ligand were circulated for another 3 min (tracer incubation time). After 10 min the pump was stopped, and aliquots were taken and measured in a γ-counter (Wizard3; Perkin-Elmer). The thrombus was removed together with the roughened thread from the thrombus chamber, and both were rinsed with saline, measured in a γ-counter, dried, and weighed. In some studies, the calcified blood was exchanged with buffer or fresh blood after 3 min of tracer incubation to simulate tracer washout conditions.

The impact of anticoagulants on ^{18}F-GP1 thrombus binding was investigated with blood from a donor, who had taken 600 mg of acetylsalicylic acid (aspirin) 24 h before investigation by the in vitro thrombus model described above. In another experiment, the blood of a donor was collected in tubes prepared with heparin (2 I.E./mL of blood). ^{99m}Tc-labeled apcitide (^{99m}Tc-Acutect) (*19*) was also investigated in this model for comparison. From each individual blood donor, multiple independent studies were performed. Studies in which clots had a weight of more than 0.1 mg were used for the calculation of clot-to-blood ratios.

In Vitro PET Study. The in vitro blood thrombus model described above was combined with a PET camera (Inveon PET/CT; Siemens) to investigate the capability to image ^{18}F-GP1 thrombus binding. The part of the tube set that contained the thrombus was placed inside the PET camera. The thrombus was imaged continuously from the addition of the tracer up to 60 min after injection. To simulate tracer washout conditions, 3 min after tracer incubation the blood was exchanged with new citrated blood after 10 min. In 1 set of experiments, excess nonradioactive ^{19}F-GP1 (2.8 μM) was added after 30 min to study displacement.

PET Imaging Studies in Cynomolgus Monkeys

The animals were handled in compliance with German animal welfare legislation, and the experiments were performed with the approval of the state animal welfare committee. In vivo binding studies were performed in cynomolgus monkeys (*Macaca fascicularis*, female, R.C. Hartelust BV, $n = 3$). Before interventions, the animals were anesthetized with an intramuscular injection of a mixture of xylazin (0.12 mL/kg; Rompun [Bayer Healthcare]) and ketamine (0.12 mL/kg; Ketavet [Pfizer]). Buprenorphine (6 μg/kg) was administered intramuscularly as analgesia.

A roughened polyethylene tube was advanced into either the thoracic aorta via the carotid artery or the vena cava via the femoral vein 30 min before tracer administration. The animals were placed inside the PET camera (Inveon PET/CT; Siemens) and 25 MBq/

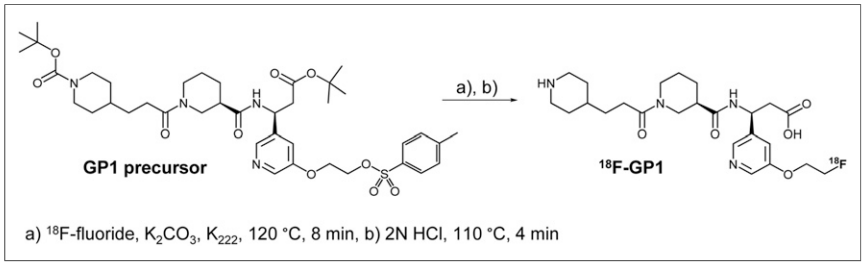

FIGURE 1. Radiosynthesis of ^{18}F-GP1 was performed starting from Boc-protected tosylate precursor (GP1 precursor). A 2-step synthesis followed by purification afforded 1.8–3.5 GBq of ^{18}F-GP1 (yield, 39% ± 4% decay corrected; radiochemical purity > 99%) in 81–84 min overall preparation time ($n = 3$).

animal of ^{18}F-GP1 were administered intravenously. Dynamic PET images of the thorax were acquired from 0 to 60 min after injection. Subsequently, static images of the brain and the lower abdomen were acquired for 10 min. After the PET data acquisition was finished, the catheter was removed and the thrombus was weighed and counted in the γ-counter. The animals were sacrificed by phenobarbital treatment before recovery from anesthesia. For organ distribution, parts of all important organs (liver, kidney, lung, spleen) and body fluids (blood, gall, urine) were removed and weighed and the activity determined with a γ-counter. PET data were reconstructed using the 2-dimensional ordered-subset expectation maximization algorithm and analyzed with the software package provided by the scanner manufacturer. A 3-dimensional volume of interest was manually drawn for quantification of uptake and kinetic analyses.

RESULTS

In Vitro Characterization of ^{19}F-GP1 and ^{18}F-GP1

^{19}F-GP1 bound to purified human GPIIb/IIIa receptor with an IC_{50} value of 20 nM in a competition assay against ^{3}H-elarofiban (Fig. 2A). An IC_{50} of 19 nM was measured for elarofiban in the same assay. The inhibition of platelet aggregation was investigated using human platelet-rich plasma. In this assay, an IC_{50} of 43 nM was determined for tirofiban and 147 nM for ^{19}F-GP1 (Supplemental Fig. 1; supplemental materials are available at http://jnm.snmjournals.org). The ability of ^{18}F-GP1 to bind to an explanted human thrombus from the left ventricle was analyzed by autoradiography. After incubation with ^{18}F-GP1, a strong signal bound to the thrombus was observed that can be fully displaced by competition with excess GPIIb/IIIa ligand. CD41 (GPIIb) staining of the slices confirmed that ^{18}F-GP1 bound in regions with cellular platelet deposition (Fig. 2B).

Because binding to isolated receptors and on tissue slides is static, the binding characteristics of ^{18}F-GP1 were investigated during circulation in a less artificial environment. An in vitro blood flow model was established, allowing thrombus formation under standardized conditions (Figs. 3A and 3B). In this model, ^{18}F-GP1 showed a strong accumulation at the site of thrombus formation. The binding was specific and could be blocked by addition of an excess of elarofiban. Clots in this model were CD41-positive by immunohistochemistry (data not shown). The average clot-to-blood ratio was 95.2 ± 50.2 for ^{18}F-GP1 and 35.2 ± 17.6 for apcitide (Fig. 3C). The impact of therapeutics to prevent blood clots (e.g., aspirin and heparin) on ^{18}F-GP1 binding to thrombi was examined in the in vitro thrombus model. ^{18}F-GP1 still bound strongly and specifically to thrombi despite the pretreatment with heparin or aspirin. The clot-to-blood ratio was significantly different between unblocked and blocked ($P < 0.01$) under all conditions studied as shown by an unpaired t test.

The binding characteristics of ^{18}F-GP1 were further analyzed in the blood flow model by continuous signal detection using a PET camera. Immediately after tracer addition, a signal at the thrombus site was measured, increasing throughout the 3-min tracer circulation time frame. The signal at the thrombi remained over the entire imaging period (Fig. 4). In 1 set of experiments, excess nonradioactive ^{19}F-GP1 was added to the circuit at 30 min and thrombus-bound radioactivity was abolished over the next 30 min.

Cynomolgus Monkey PET Imaging

Biodistribution analysis in cynomolgus monkeys showed rapid clearance of ^{18}F-GP1 from healthy tissues and the blood. The tracer concentration measured in the aorta by PET was in good agreement with the activity measured in blood samples. After the

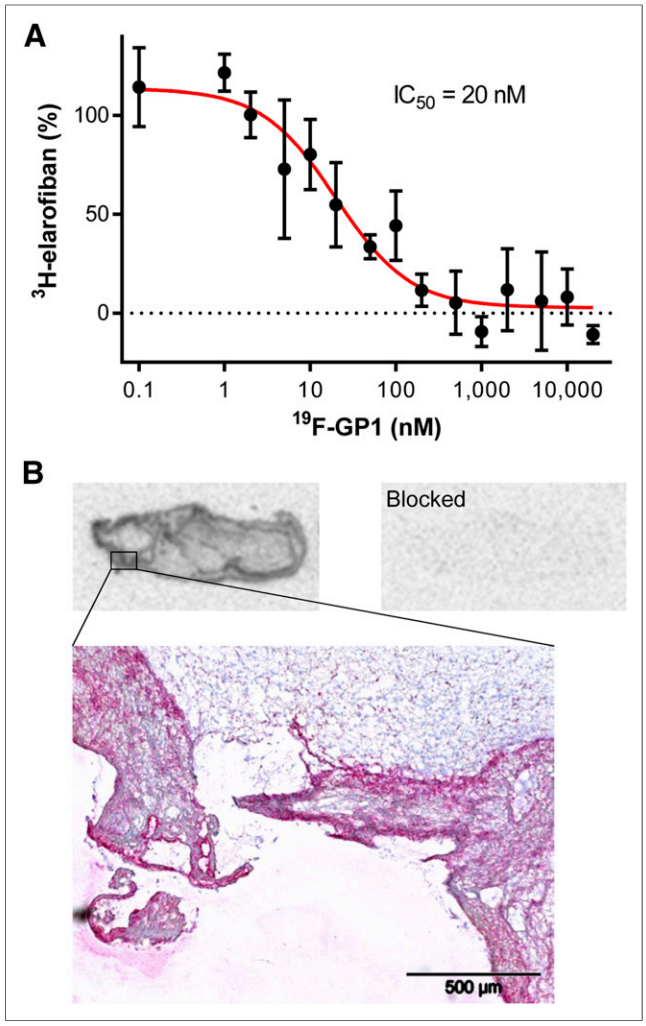

FIGURE 2. Binding characteristics of ^{19}F-GP1 and ^{18}F-GP1. (A) IC_{50} measurement of nonradioactive ^{19}F-GP1 derivative on microtiter plates coated with human GPIIa/IIIb. (B) Autoradiography using ^{18}F-GP1 on slice of clinical left ventricular thrombus explanted from human heart. CD41 (GPIIb) staining is shown below.

imaging study was finished, at 60 min after injection the animals were sacrificed and an ex vivo organ distribution analysis was performed. Low organ uptake was observed except the gallbladder (Supplemental Figs. 2A and 2B). The maximum-intensity projection of summed frames from the thorax region obtained directly after injection (0–5 min) visualized the activity in the main blood vessels. At later time points (40–60 min), no detectable signal was observed in the thorax (Supplemental Figs. 2C and 2D).

For the in vivo thrombus imaging, a catheter with a roughened thrombogenic area was placed into the left carotid artery of cynomolgus monkeys as shown in a schematic illustration (Fig. 5A). The PET images obtained from all 3 animals examined revealed a strong signal inside the descending aorta along the roughened part of the catheter, with no visible signal associated with the nonroughened catheter and only a sparse signal in the surrounding tissues (Fig. 5B). After removal of the catheters from the animals, a thin layer of thrombi covering the roughened part of the catheter was observed. The thrombogenic volume (1-cm length × 0.2-cm diameter, ~30 μL) indicates that the method allows for detection of even small thrombi with high detection sensitivity. No comparison

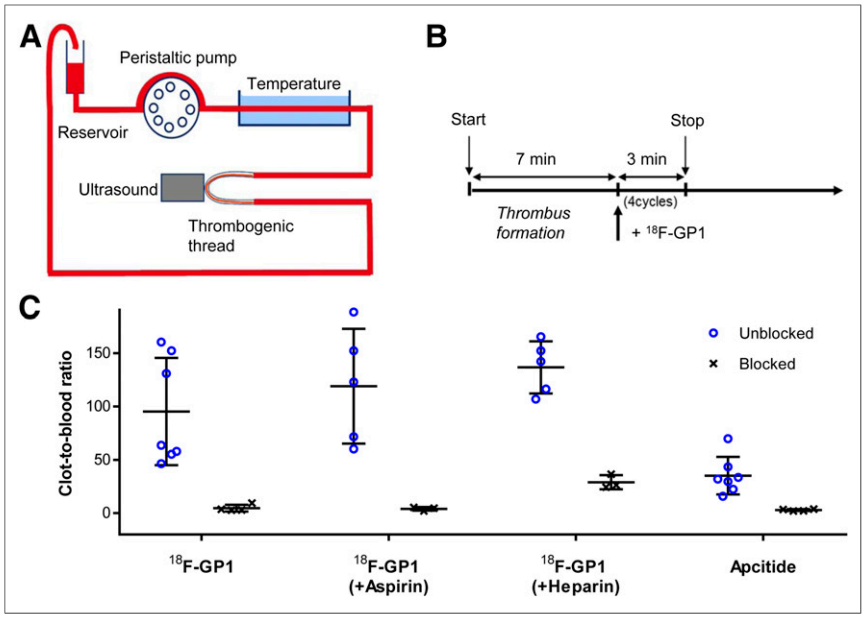

FIGURE 3. Determination of clot-to-blood ratios using in vitro blood flow model. (A) Experimental setup. (B) Sequence and duration of steps. (C) Clot-to-blood ratios were determined for ^{18}F-GP1 and apcitide under different conditions. Clot-to-blood ratio was significantly different between unblocked and blocked under all conditions studied as shown by an unpaired *t* test ($P < 0.01$).

with other standard imaging techniques such as CT, pulmonary angiography, or ultrasonography was performed in this study. A signal inside the brain was anecdotally noted when other parts of the body were scanned after the 60-min dynamic scan of the thorax was finished (Fig. 5C). Autopsy revealed a thrombus within the internal carotid artery/Circle of Willis junction (Fig. 5D). It remains unclear if this thrombus detached from the aortic thrombus at the beginning of the experiment (before tracer injection) or at the end of the experiment (after tracer injection). Therefore, it is not yet confirmed that ^{18}F-GP1 can target emboli in the brain; however, the profound spatial resolution was confirmed. In the other studied monkeys, the brains were completely free of any signal. Additional studies are required to assess whether thromboembolic events can be imaged in animal models or humans.

Through insertion of catheters into the right carotid artery and into the vena cava, arterial and venous thrombi were induced in cynomolgus monkeys. Both, the arterial and the venous thrombi were equally visualized by ^{18}F-GP1 PET imaging, with almost no background from any organ or tissue in the field of view (Fig. 6A). A thin layer of thrombus formation was observed at the roughened areas that showed the same pattern as the PET signals. In the animal shown, the left carotid artery was accidentally injured during the insertion of the catheter into the left jugular vein. This caused an endothelial damage that was confirmed at necropsy. The resulting small thrombotic depositions at the damaged endothelial surface were clearly visualized in vivo in the PET image. Although unintended, this observation emphasizes that ^{18}F-GP1 is capable of visualizing small arterial thrombi, formed in situ within a monkey carotid artery. Time–activity curves confirmed stable binding to both arterial and venous thrombi throughout the 60-min dynamic scan (Fig. 6B).

DISCUSSION

The development of high-affinity, rapidly clearing radiolabeled small molecules targeting GPIIb/IIIa together with the recent advances in PET imaging technologies provide an opportunity to overcome the limitations of the previously introduced SPECT agents by detecting thrombi with improved spatial resolution and detection sensitivity. The elarofiban scaffold was selected on the basis of suitable pharmacokinetic properties and feasibility for incorporating the ^{18}F radiolabel without losing biologic activity. Binding studies with either purified GPIIb/IIIa or human thrombus showed that modification of elarofiban with a small fluoro-containing moiety did not affect the binding affinity. In fact, the ^{19}F-GP1 derivative showed in this competition assay an IC_{50} value similar to the parent elarofiban molecule. The measured IC_{50} value of the parent elarofiban in this assay was higher than its reported IC_{50} value using biotinylated fibrinogen in a competition assay (0.4 nM) (*13*). Because different ligands and conditions were applied, these values cannot be directly compared but it can be concluded that the high affinity of elarofiban for GPIIb/IIIa is retained for ^{18}F-GP1.

Species differences in the ligand binding to the GPIIb/IIIa receptors are reported in the literature (*13,16,25,26*), and rodents were shown to be not appropriate for the in vivo evaluation of this class of new receptor ligands. Species-dependent effects are also reported for elarofiban, necessitating the use of human blood or thrombi for binding studies and autoradiography as well as establishing a nonhuman primate model for PET imaging of thrombi. Moderate inhibition of platelet aggregation was observed with ^{19}F-GP1. The very low mass dose (<10 μg per dose) applied for radiotracer imaging would result in an initial blood concentration in humans that will be more than 50-fold below the IC_{50} for aggregation inhibition.

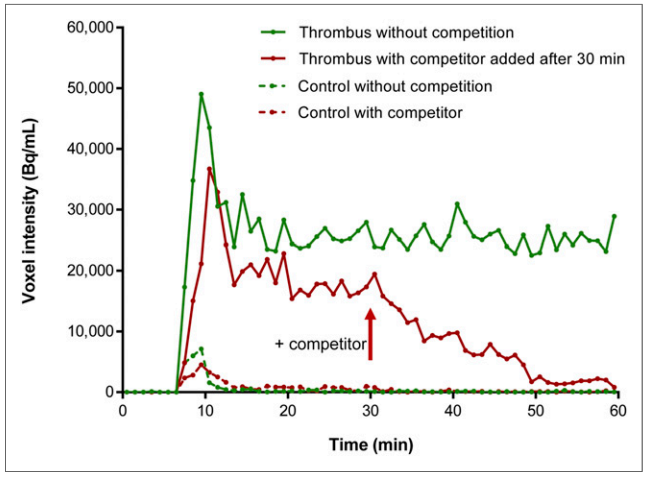

FIGURE 4. PET imaging of ^{18}F-GP1 thrombus binding in in vitro blood flow model (representative time–activity curves shown). Strong signal was measured in thrombus region directly after tracer addition at 7 min whereas low signal was measured in control area (dashed lines). ^{18}F-GP1 remained bound to thrombus over whole imaging procedure. After addition of excess nonradioactive ^{19}F-GP1 at 30 min, complete displacement of thrombus-bound signal was observed until 60 min.

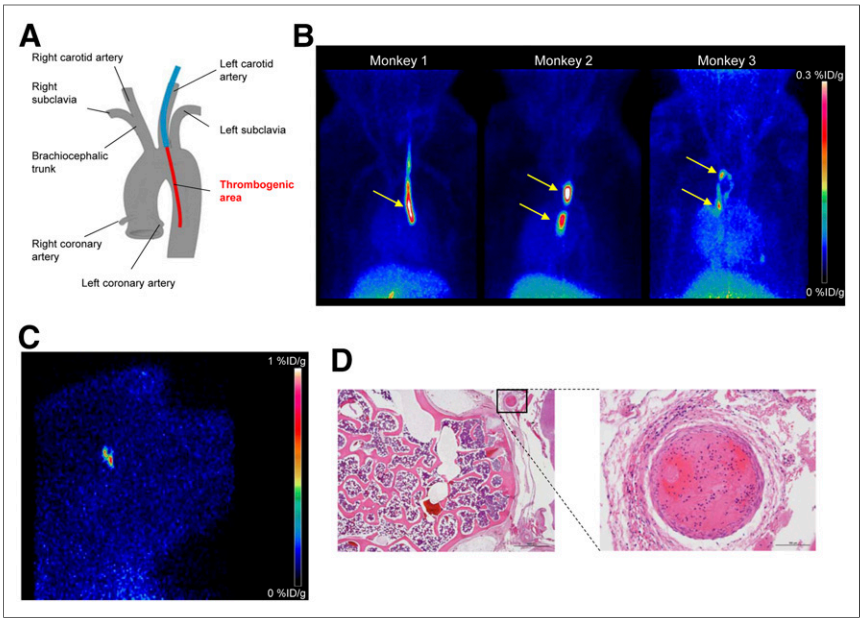

FIGURE 5. PET imaging of arterial thrombi with ^{18}F-GP1 in cynomolgus monkeys. (A) Schematic illustration of location of advanced catheter in descending aorta. (B) PET images (maximum-intensity projection, 0–60 min) of 3 cynomolgus monkeys. Strong signals are detected at sites in which catheters with roughened surfaces were introduced. Almost no other background signal is visible. Only accumulation in gallbladder becomes visible at bottom of image. (C) Suspect PET imaging finding inside brain of monkey 2 measured after 60-min dynamic scanning of thorax. (D) Finding observed in C was confirmed as thrombus inside internal carotid artery/Circle of Willis junction by pathology. %ID/g = percentage injected dose per gram.

Together with the rapid tracer clearance this makes bleeding adverse events extremely unlikely.

An important consideration, which is not addressed well enough in the applied in vitro and in vivo models, is the target specificity of the current compound compared with previous RGD mimetics. It has been shown that cyclic RGD compounds bind to GPIIb/IIIa as well as other integrins, particularly $\alpha_v\beta_3$. The target $\alpha_v\beta_3$ is present on activated endothelial cells and smooth muscle cells. Other integrins are present on inflammatory cells. This may explain why agents such as apcitide show a diffuse soft-tissue uptake in the vicinity of the DVT. Elarofiban has shown a more than 300,000-fold specificity for GPIIb/IIIa over $\alpha_v\beta_3$ (*27*), and it can be postulated that the thrombus is better visualized using an elarofiban derivative without obfuscation by the surrounding inflamed tissue in humans. Higher target specificity should also allow a more accurate detection of pathologic mechanisms in atherosclerosis where both platelets and vascular cells are implicated. In principle it will also improve the discrimination between infectious and thrombogenic events (e.g., endocarditis, valvular vegetations), although this has yet to be tested.

The human ex vivo blood circuit is a simple model to study clot formation in vitro and is flexible, allowing investigations of different blood species, anticoagulants, and flow rates. Coupling the blood circuit to a PET camera allows real-time quantification of clot binding and retention. Especially measurements under arterial flow rates were used to maximize the adhesion of activated platelets. The combined results of abrogation of tracer binding to the clot by addition of excess unlabeled GP1 or elarofiban and unaffected clot accumulation of ^{18}F-GP1 under aspirin or heparin treatment confirm specific tracer binding. Real-time assessment when the nidus was placed inside a PET camera recapitulated the results and, furthermore, confirmed the rapid accumulation and visualization of the retained ^{18}F-GP1 on the clot.

Preclinical proof of in vivo thrombus imaging was obtained after insertion of analogously prepared roughened polyethylene catheters into the primate arterial system and into the venous system. Even small thrombi were easily and distinctly visualized at the roughened catheter region. The ability to image small thrombi was confirmed by the observation in 1 animal in which the carotid artery was inadvertently damaged during catheter placement. This recapitulated a real-life situation and showed that ^{18}F-GP1 was able to visualize naturally occurring thrombi. The intracerebral clot visualization was opportunistic but gave insight into the possible capabilities of ^{18}F-GP1. It is unknown whether ^{18}F-GP1 was injected before or after the arterial thrombus was displaced and lodged in the brain. Nonetheless, it represents the visualization of a small clot lodged in the middle cerebral artery and bodes well for the possibility of imaging strokes/cerebrovascular accidents in humans.

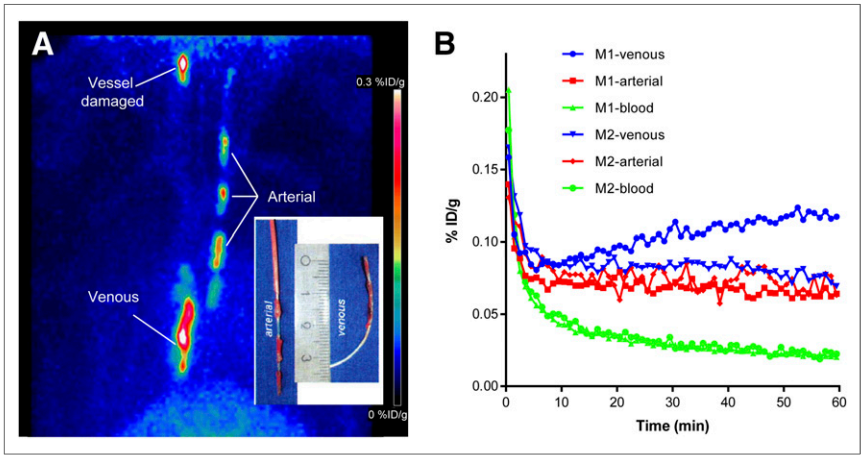

FIGURE 6. (A) ^{18}F-GP1 PET image (maximum-intensity projection, 0–60 min) of cynomolgus monkey with arterial and venous catheter that were introduced in right carotid artery and into vena cava, respectively. Tracer uptake was visualized in both arterial and venous thrombi in both animals investigated with 2 catheters. (B) Time–activity curves of ^{18}F-GP1 thrombus uptake and blood clearance from monkey 1 shown in A and monkey 2. %ID/g = percentage injected dose per gram.

CONCLUSION

^{18}F-GP1 is a promising novel PET tracer for thrombus imaging in vitro and in vivo. It binds with high affinity to GPIIb/IIIa, the key receptor for platelet

aggregation. Strong binding was observed on an explanted human cardiac thrombus, in the in vitro human blood flow–thrombus model, and on platelet depositions on catheter and endothelium surfaces as well as on emboli in cynomolgus monkeys, confirming its potential for PET imaging of such thrombogenic events. Efficacy was not altered by anticoagulation therapy. A favorable biodistribution profile supports the translation of ^{18}F-GP1 into the clinic. A first-in-human study is currently ongoing and further conclusions await clinical trial results.

DISCLOSURE

This work was funded by Bayer Pharma AG and Piramal Imaging GmbH, Berlin, Germany. Andrew Stephens, Mathias Berndt, Andre Müller, Norman Koglin, Felix Oden, Marion Zerna, Matthias Friebe, and Ludger Dinkelborg are employees of Piramal Imaging GmbH, Berlin, Germany. Jessica Lohrke, Holger Siebeneicher, Markus Berger, Marcus Bauser, and Joachim Hütter are employees of Bayer Pharma AG, Berlin, Germany. No other potential conflict of interest relevant to this article was reported.

ACKNOWLEDGMENTS

We thank Robert Ivkic, Martin Kohs, Violetta Sudmann, Lorenz Behringer, and Samira Leesch for their motivation, excellent work, and skilled technical assistance. Furthermore, we thank Anna-Lena Frisk for performing histopathology examinations and the Heart and Diabetes Center Bad Oeynhausen for providing an explanted human thrombus. The platelet aggregation data were kindly provided by Christoph Gerdes (TRG Cardiology, Bayer Pharma, Wuppertal).

REFERENCES

1. Mozaffarian D, Benjamin EJ, Go AS, et al. Heart disease and stroke statistics-2016 update: a report from the American Heart Association. *Circulation.* 2016;133:e38–e360.
2. Pomero F, Dentali F, Borretta V, et al. Accuracy of emergency physician-performed ultrasonography in the diagnosis of deep-vein thrombosis: a systematic review and meta-analysis. *Thromb Haemost.* 2013;109:137–145.
3. Lee W. General principles of carotid Doppler ultrasonography. *Ultrasonography.* 2014;33:11–17.
4. Srichai MB, Junor C, Rodriguez LL, et al. Clinical, imaging, and pathological characteristics of left ventricular thrombus: a comparison of contrast-enhanced magnetic resonance imaging, transthoracic echocardiography, and transesophageal echocardiography with surgical or pathological validation. *Am Heart J.* 2006;152:75–84.
5. Fedullo PF, Tapson VF. Clinical practice. The evaluation of suspected pulmonary embolism. *N Engl J Med.* 2003;349:1247–1256.
6. Righini M, Le Gal G, Aujesky D, et al. Diagnosis of pulmonary embolism by multidetector CT alone or combined with venous ultrasonography of the leg: a randomised non-inferiority trial. *Lancet.* 2008;371:1343–1352.
7. Ciesienski KL, Caravan P. Molecular MRI of thrombosis. *Curr Cardiovasc Imaging Rep.* 2010;4:77–84.
8. Zierler BK. Ultrasonography and diagnosis of venous thromboembolism. *Circulation.* 2004;109:I9–I14.
9. Stein PD, Fowler SE, Goodman LR, et al. Multidetector computed tomography for acute pulmonary embolism. *N Engl J Med.* 2006;354:2317–2327.
10. Sweet PH 3rd, Armstrong T, Chen J, Masliah E, Witucki P. Fatal pulmonary embolism update: 10 years of autopsy experience at an academic medical center. *JRSM Short Rep.* 2013;4:2042533313489824.
11. Nurden P, Poujol C, Durrieu-Jais C, et al. Labeling of the internal pool of GP IIb-IIIa in platelets by c7E3 Fab fragments (abciximab): flow and endocytic mechanisms contribute to the transport. *Blood.* 1999;93:1622–1633.
12. Cook JJ, Bednar B, Lynch JJ, et al. Tirofiban (Aggrastat®). *Cardiovasc Drug Rev.* 1999;17:199–224.
13. Damiano BP, Mitchell JA, Giardino E, et al. Antiplatelet and antithrombotic activity of RWJ-53308, a novel orally active glycoprotein IIb/IIIa antagonist. *Thromb Res.* 2001;104:113–126.
14. Hoekstra WJ, Beavers MP, Andrade-Gordon P, et al. Design and evaluation of nonpeptide fibrinogen gamma-chain based GPIIb/IIIa antagonists. *J Med Chem.* 1995;38:1582–1592.
15. Hoekstra WJ, Maryanoff BE, Damiano BP, et al. Potent, orally active GPIIb/IIIa antagonists containing a nipecotic acid subunit: structure-activity studies leading to the discovery of RWJ-53308. *J Med Chem.* 1999;42:5254–5265.
16. Maryanoff BE. Adventures in drug discovery: potent agents based on ligands for cell-surface receptors. *Acc Chem Res.* 2006;39:831–840.
17. Scarborough RM, Gretler DD. Platelet glycoprotein IIb-IIIa antagonists as prototypical integrin blockers: novel parenteral and potential oral antithrombotic agents. *J Med Chem.* 2000;43:3453–3473.
18. Houshmand S, Salavati A, Hess S, Ravina M, Alavi A. The role of molecular imaging in diagnosis of deep vein thrombosis. *Am J Nucl Med Mol Imaging.* 2014;4:406–425.
19. Lister-James J, Knight LC, Maurer AH, Bush LR, Moyer BR, Dean RT. Thrombus imaging with a technetium-99m-labeled activated platelet receptor-binding peptide. *J Nucl Med.* 1996;37:775–781.
20. Douketis JD, Ginsberg JS, Haley S, et al. Accuracy and safety of ^{99m}Tc-labeled anti-D-dimer (DI-80B3) Fab' fragments (ThromboView(R)) in the diagnosis of deep vein thrombosis: a phase II study. *Thromb Res.* 2012;130:381–389.
21. Morris TA, Gerometta M, Yusen RD, et al. Detection of pulmonary emboli with ^{99m}Tc-labeled anti-D-dimer (DI-80B3)Fab' fragments (ThromboView). *Am J Respir Crit Care Med.* 2011;184:708–714.
22. Blasi F, Oliveira BL, Rietz TA, et al. Radiation dosimetry of the fibrin-binding probe ^{64}Cu-FBP8 and its feasibility for PET imaging of deep vein thrombosis and pulmonary embolism in rats. *J Nucl Med.* 2015;56:1088–1093.
23. Breddin HK. Can platelet aggregometry be standardized? *Platelets.* 2005;16:151–158.
24. Sukavaneshvar S. Assessment and management of vascular implant thrombogenecity. In: Wakhloo AK GM, Lieber BB, eds. *Thrombus and Stroke.* New York, NY: Informa Healthcare; 2008:57–77.
25. Basani RB, Zhu H, Thornton MA, et al. Species differences in small molecule binding to alpha IIb beta 3 are the result of sequence differences in 2 loops of the alpha IIb beta propeller. *Blood.* 2009;113:902–910.
26. Harfenist EJ, Packham MA, Mustard JF. Effects of the cell adhesion peptide, Arg-Gly-Asp-Ser, on responses of washed platelets from humans, rabbits, and rats. *Blood.* 1988;71:132–136.
27. De Corte BL, Kinney WA, Liu L, et al. Piperidine-containing beta-arylpropionic acids as potent antagonists of alphavbeta3/alphavbeta5 integrins. *Bioorg Med Chem Lett.* 2004;14:5227–5232.